Stratospheric Gravity Waves as a Proxy for Hurricane Intensification: a Case Study of WRF Simulation for Hurricane Joaquin

Xue Wu[1, 6], Lars Hoffmann[2], Corwin J. Wright[3], Neil P. Hindley[3], Silvio Kalisch[4], M. Joan Alexander[5], and Yinan Wang[1]

[1]Key Laboratory of Middle Atmosphere and Global Environment Observation, Institute of Atmospheric Physics, Chinese Academy of Sciences, Beijing, China

[2]Jülich Supercomputing Centre, Forschungszentrum Jülich, Jülich, Germany

[3]Centre for Space, Atmospheric and Oceanic Science, University of Bath, Bath, UK

[4]Department of Atmospheric Sciences, Yonsei University, Seoul, South Korea

[5]NorthWest Research Associates, CoRA Office, Boulder, CO, USA

[6]University of Chinese Academy of Sciences, Beijing, China

Corresponding authors: Xue Wu (wuxue@mail.iap.ac.cn) and Lars Hoffmann (l.hoffmann@fz-juelich.de)

Key Points:

- High-resolution WRF simulations for Hurricane Joaquin show spiral gravity waves (GWs) emanating into the stratosphere.
- Stratospheric GW activity is more frequent and intense before and during hurricane intensification than during weakening.
- This study provides further evidence that stratospheric GW activity is a valid proxy for hurricane intensification.

Abstract

We conducted simulations with a 4-km resolution for Hurricane Joaquin in 2015 using the Weather Research and Forecast (WRF) model. The model data are used to study stratospheric gravity waves (GWs) generated by the hurricane and how they correlate with hurricane intensity. The simulation results show spiral GWs propagating upward and anticlockwise away from the hurricane center. GWs with vertical wavelengths up to 14 km are generated. We find that GW activity is more frequent and intense during hurricane intensification than during weakening, particularly for the most intense GW activity. There are significant correlations between the change of stratospheric GW intensity and hurricane intensity. Therefore, the emergence of intensive stratospheric GW activity may be considered a useful proxy for identifying hurricane intensification.

Plain Language Summary

Accurate predictions of changes in hurricane intensity are essential to provide sufficient lead time for warning and evacuation. As a hurricane intensifies, gravity waves (GWs) are emitted into the stratosphere to partially rebalance the sudden energy changes. If a correlation between hurricane intensification and GWs is verified, observing stratospheric GWs with satellite instruments could provide a possible predictor of hurricane intensification. This approach is advantageous when clouds obscure the direct view from above by visible and infrared instruments into the inner state of the hurricane. This study uses mesoscale model simulations to test and verify the correlation between hurricane intensification and GWs and finds that stratospheric GW activity increases prior to peaks in hurricane intensity.

1 Introduction

Tropical cyclones (TCs) are among the most destructive natural weather phenomena and can cause extensive damage to coastal countries and regions. Close monitoring and accurate forecasts of the tracks and intensity of TCs are needed to reduce human and financial losses.

Tropical cyclones are powered by latent heating, mainly from strong updrafts in the eyewall (Charney and Eliassen, 1964; Emanuel, 1986; Kuo, 1965), and latent heat release in the storm is responsible for the dynamical structure and intensity change of the storm (Braun, 2002; Cecil and Zipser, 1999). Latent heat release is also involved in generating stratospheric gravity waves (GWs) (Beres et al., 2004; Song and Chun, 2005; Kuester et al., 2008). Previous studies found a dependence of dominant phase speed and wavelengths of GWs on the depth of the latent heating in the troposphere (e.g., Alexander et al., 1995; Beres et al., 2002, 2004; Salby and Garcia, 1987). Thus, the spatial scale and temporal variation of heating rate determine the spectrum of GWs in the stratosphere (e.g., Alexander and Holton, 2004; Holton et al., 2002; Nicholls et al., 1991; Stephan and Alexander, 2015). Ground-based and satellite observations, reanalysis data, and model simulations have been widely used to study the characteristics of stratospheric GWs generated by convective systems, particularly TCs (e.g., Chane-Ming et al., 2010, 2019; Chow et al., 2002; Kim and Chun, 2010; Miller et al., 2015; Nolan and Zhang, 2017; Wu et al., 2018; Yue et al., 2014), and confirmed that the characteristics of GWs vary significantly as the intensity of TCs changes.

Since stratospheric GW activity and TC intensity change are both driven by heating, recent works have suggested stratospheric GWs can be used as a proxy for intensity change (Hoffmann et al., 2018; Tratt et al., 2018). Model simulations have revealed that strong updrafts or convective bursts appear up to 3 h before TC intensification (Hazelton et al., 2017). GWs with long vertical wavelengths generated by the deep latent heat can propagate to the stratosphere in less than one hour (Fritts and Alexander, 2003; Yue et al., 2013, 2014), and this means that intensive stratospheric GW activity could be a predictor for TC intensification on short-term time scales. Using 13.5 years of Atmospheric Infrared Sounder (AIRS) observations of stratospheric GWs, Hoffmann et al. (2018) found a statistically robust correlation that more intensive stratospheric GWs are observed during the intensification of TCs than during weakening. Wright (2019) presented a study of TC-induced GWs using the Microwave Limb Sounder (MLS), the Sounding of the Atmosphere using Broadband

Emission Radiometry (SABER), and the High-Resolution Dynamics Limb Sounder (HIRDLS). Despite different GW spectrum ranges revealed by the sounders, Wright (2019) found a similar result that GW amplitudes steadily increase before TCs reaching peak intensity. However, these relationships require further verification due to the coarse time and space sampling of these satellite observations.

Following the work of Hoffmann et al. (2018), this study conducts realistic model simulations of stratospheric GWs generated by hurricane Juaquin in 2015 to verify the statistical correlation revealed by long-term satellite observations and to examine the possibility to use GW activity as a proxy of hurricane intensity change.

2 Reanalysis and observational data

2.1 ERA5 reanalysis

In this study, we use ERA5 reanalysis data (Hersbach et al., 2020) to provide initial and boundary conditions for the WRF simulation of Hurricane Joaquin. The ERA5 reanalysis is produced using the European Centre for Medium-Range Weather Forecasts (ECMWF) IFS Cycle 41r2 model with 4D-Var data assimilation and has a horizontal resolution of 31 km (T_L639 spectral grid). The data are provided at 137 vertical hybrid sigma-pressure levels with the top level at 0.01 hPa (~80 km) as well as at the surface level. We retrieved hourly data at 0.25° × 0.25° horizontal sampling and all model levels from the ECMWF data archive. Although tropical cyclone intensities are often underestimated in earlier reanalyses (Hodges et al., 2017), ERA5 better resolves mesoscale vertical motions both over the land and near the Intertropical Convergence Zone (ITCZ) (Hoffmann et al., 2019), which provides more accurate initial and boundary conditions for the simulations of hurricane intensity.

2.2 Tropical cyclone track and intensity archive

The International Best Track Archive for Climate Stewardship (IBTrACS) (Knapp et al., 2010) was used to evaluate the track and intensity of Hurricane Joaquin in our model simulations. The IBTrACS data were compiled from Regional Specialized Meteorological Centers within the World Meteorological Organization and other national agencies, which compile and archive TC track data individually. The IBTrACS data provides 3 to 6-hourly track and intensity estimates of hurricanes.

3 WRF model configuration

Successful reproduction of the TC track and intensity is crucial for simulating and evaluating the TC-induced GWs. A numerical simulation of Hurricane Joaquin was performed using the Weather Research and Forecasting (WRF) model version 3.9.1 (Skamarock et al., 2008). To adequately reproduce the rapid intensification phase of Hurricane Joaquin, it is necessary to conduct simulations with sufficient horizontal resolution. Horizontal resolutions coarser than 3–4 km may fail to represent the physical processes critical to TC intensity evolution (Gentry and Lackmann, 2010; Kim and Chun, 2010). In this study, the simulation used a concurrent one-way nested configuration that featured a fixed outer domain (D01) with 210×105 grid points and a vortex-following inner nested domain (D02) with 201×201 grid points. The repositioning of D02 was calculated every 15 min. The grid spacings for D01 and

D02 are 12 and 4 km, and the time steps for D01 and D02 are 12 s and 4 s, respectively. A vertical domain with 90 sigma levels was set from the surface up to 1 hPa (~49 km), and the topmost 5 km was established as a damping layer. The vertical grid spacing was about 500 m in the stratosphere. The simulation spans 100 h from 00:00 UTC 30 September to 04:00 UTC 4 October 2015, and simulation outputs were stored every 6 min.

Initial and boundary conditions were established using the ERA5 reanalysis data. For both domains, the Kain-Fritsch scheme (Kain, 2004) for cumulus parameterization, the WRF single moment 6-class scheme (Hong and Lim, 2006) for microphysics, the new version of rapid radiative transfer model scheme (Iacono et al., 2008) for longwave and shortwave radiation, and the Yonsei University planetary boundary layer scheme (Hong et al., 2006) for the vertical diffusion process were applied. As in Kim and Chun (2010), GWs structures are not fully represented in model outputs from D01, so we emphasize analyzing the outputs from D02. D01 is only used to provide initial and lateral boundary conditions for the vortex-following D02.

4 Results

4.1 WRF-simulated track and intensity of Hurricane Joaquin

Figure 1a shows the geographic region covered by D01 and the initial location of D02, and compares the WRF-simulated hurricane track with the hurricane track provided by IBTrACS. The WRF-simulated hurricane track reproduced the slow southwestward movement of Joaquin before it stalled near the Bahamas and eventually accelerated northeastward. Figure 1b,c compares the time series of hurricane intensity, represented by IBTrACS maximum sustained wind speed (MSW), versus maximum surface wind speed from the WRF simulation (referred to as MSFCW hereafter) and the IBTrACS versus WRF simulated minimum sea level pressure (MSLP). After a spin-up time of about 12 h, the simulation results generally represent the hurricane intensity evolution well. Rapid intensification (i.e., MSW's change exceeding 15.4 m/s during 24 h) is well reproduced until 18:00 UTC 1 October. The simulation results also reproduce the subsequent weakening, re-intensification, and second weakening of the hurricane. Please refer to the supplement for the verification of model parameters related to latent heating.

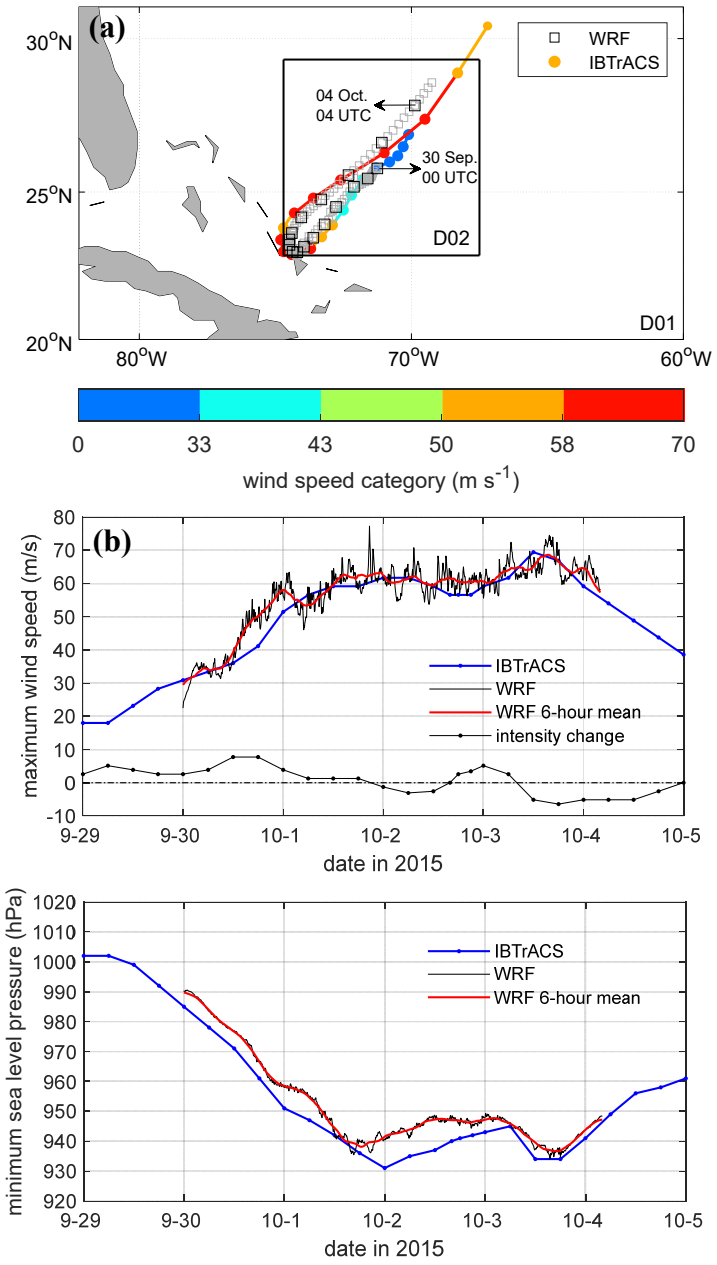

Figure 1. Comparison of the track and intensity of Hurricane Joaquin from WRF model simulation and IBTrACS data. (a) shows the hourly IBTrACS hurricane center positions (dots) from 00 UTC 29 September to 12 UTC 4 October, and WRF-simulated hurricane centers (squares) from 00 UTC 30 September to 04 UTC 4 October 2015, respectively. (b) Comparison of IBTrACS MSW and WRF-simulated MSFCW, where the 6-hourly intensity change is derived from IBTrACS data. (c) Comparison of IBTrACS and WRF simulated MSLP. In (b) and (c), the thin black lines indicate model outputs every 6 min, and the thin red lines indicate the 6-h moving mean of the model outputs.

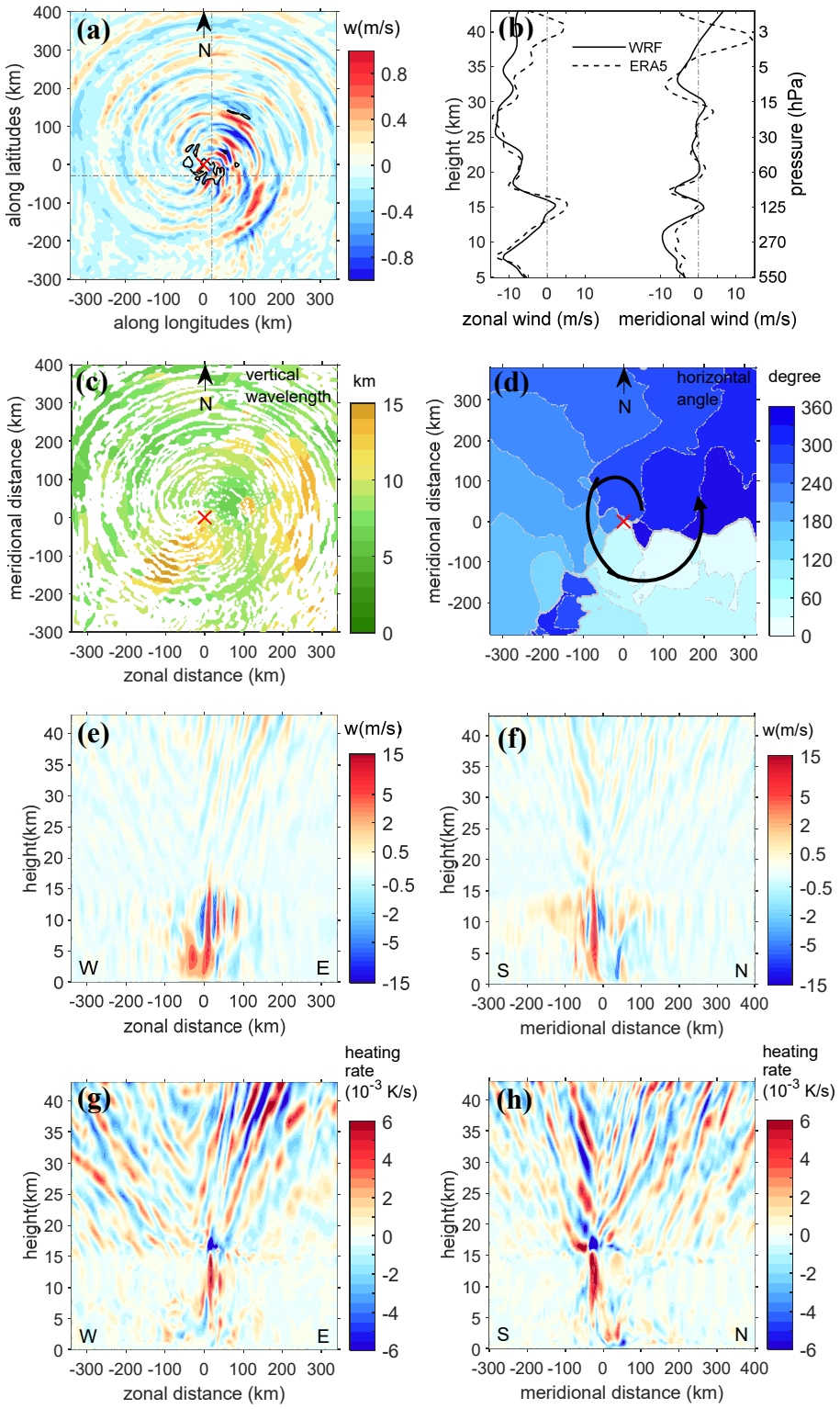

Figure 2. Features of GWs at 00:00 UTC 1 October 2015. The location of the hurricane center was 23.9°N, 72.9°W. (a) Vertical velocities at 30 km (GWs with amplitude < 0.1 m/s are excluded); the red cross denotes the hurricane center, and the black contours enclose regions where the 5–15 km net heating rate ($\partial T/\partial t$) exceed 5×10^{-4} K/s. The grey dot-dashed lines indicate the longitude and latitude the cross-sections in (e–h) are made. (b) Comparison of the simulated mean zonal and meridional wind in the inner domain with the same parameters derived from the ERA5 data. (c) Vertical wavelengths at 30 km. (d) Angles of horizontal propagation (clockwise

from north) at 30 km. The black curve with an arrow schematically shows the direction of wave propagation. (e–f) Cross-section of WRF simulated vertical velocities. (g–h) Cross-section of WRF simulated net heating rate ($\partial T/\partial t$). W: west; E: east; S: south; N: north.

4.2 Characteristics of GWs generated by Joaquin 2015

As an example of the stratospheric GWs generated by Joaquin, Fig. 2a–c shows GW features on a single level at 30 km altitude at 00:00 UTC 1 October 2015, when the hurricane was intensifying rapidly. Patterns in vertical velocity show tight spirals, similar to spiral GWs shown in the theoretical and idealized studies of Chow et al. (2002), Nolan and Zhang (2017), and Tratt et al. (2018). As seen in Fig. 2a., under the influence of the easterly flow, the GWs show asymmetric patterns: the waves are suppressed downstream on the west side of the hurricane, and the wavefronts are compacted more closely on the east side. Mean zonal and meridional winds in the inner domain are shown in Fig. 2b, and winds averaged from ERA5 data in the same area are also shown for comparison. At 30 km, the simulated mean zonal wind is about −10 m/s (i.e., easterly). GW activity and interactions with the mean flow in the 4 km WRF model output are not entirely resolved in ERA5 data at this horizontal resolution of ~31 km, and so the discrepancy between the mean winds from the model and from ERA5 increases in the stratosphere.

GW vertical wavelengths and wave propagation angles (Fig. 2c,d) are calculated by a 3D Stockwell transform method (Hindley et al., 2016, 2019; Wright et al., 2017). The wave propagation angles confirm that GWs propagate outward from the center in an anticlockwise manner. The peak vertical wavelength is about 10–14 km. As estimated from Fig. 2a, at the altitude of 30 km, the horizontal wavelengths within 200 km of the hurricane center are about 40 km. GWs with spectral characteristics such as this tend to propagate primarily vertically rather than horizontally, and as such propagation time from the troposphere to the stratosphere is usually less than 1 h (Yue et al., 2014). Strong updrafts in the upper troposphere associated with TCs produce large heating rates, also called “hot towers” (Braun et al., 2002; Montgomery et al., 2006). The tropospheric net heating rates (here defined as temperature tendency, $\partial T/\partial t$) larger than 3×10^{-3} K/s are mainly seen between 5–15 km, and net heating rates larger than 5×10^{-3} K/s between 10–15 km (Fig. 2g,h) along with the tropospheric updrafts (Fig.2e,f).

4.3 Occurrence frequency of GW events and hurricane intensity change

Figure 3 presents an analysis of stratospheric GW occurrence frequency with respect to hurricane intensity change. The WRF simulation outputs were stored every 6 min, and the GW activity sampled at a 6-min interval is referred to as one GW event hereafter. Model outputs from the spin-up period (the first 12 h) are excluded, leaving 880 events to be considered for statistical analysis. The intensity of stratospheric GWs is represented by the mean vertical velocity variance between 20 and 43 km. GW intensity varies as the hurricane intensifies and weakens. Figure 3a shows that 820 events had a vertical velocity variance larger than 0.05 m^2/s^2, 250 events had a variance larger than 0.25 m^2/s^2, and 32 events had a variance larger than 0.45 m^2/s^2. There is a clear separation in the number of GW events with respect to hurricane intensity change, with more GW events found during intensification than weakening. The distinction between intensification and weakening scenarios is particularly

clear for the strongest GW events. The ratio of GW events during hurricane intensification to GW events during hurricane weakening increases from 1.34 at the threshold of 0.05 m^2/s^2 to 2.67 at the threshold of 0.45 m^2/s^2. However, it should be kept in mind that for large variance thresholds, the ratios are calculated from smaller numbers of events, so they may exhibit larger fluctuations and uncertainties. Figure 3b shows that the probability distribution function with respect to the intensity change of the GW events is skewed toward hurricane intensification, particularly for stronger GWs.

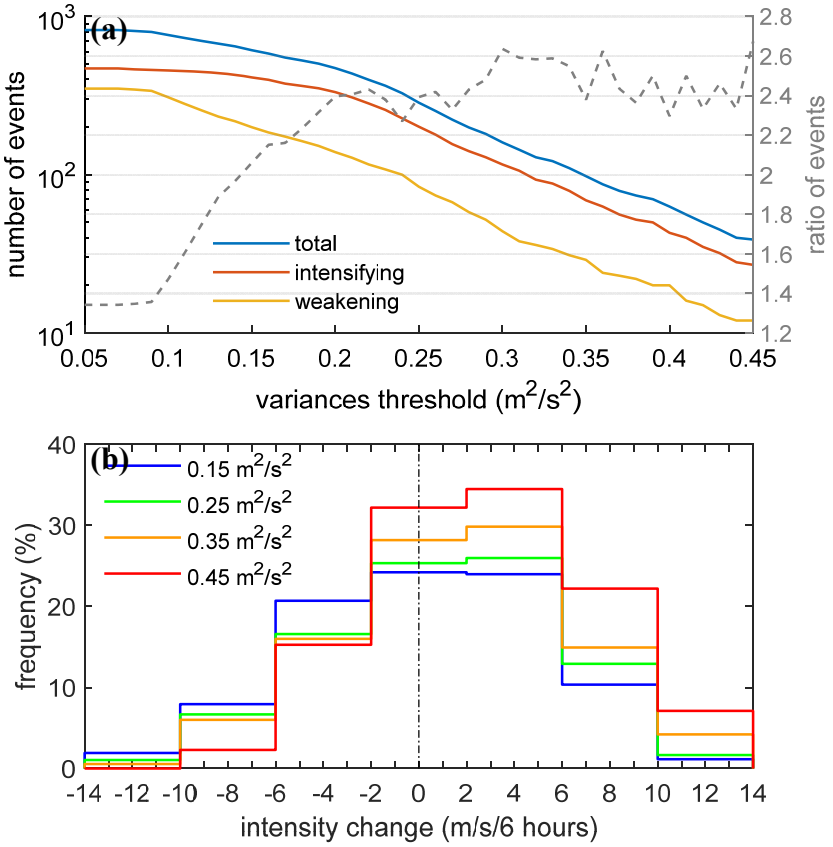

Figure 3. Occurrence frequency of stratospheric GWs with respect to the hurricane intensity change. (a) The number of GW events associated with hurricane intensification or weakening for different minimum variance thresholds and the ratios of events during hurricane intensification to events during hurricane weakening (gray dashed line). (b) Frequency distribution of GWs intensity with respect to intensity change for selected variance thresholds.

Several sensitivity tests were conducted to confirm the results above:

(i) Results are consistent whether the 6-h change of MSFCW or MSLP is used as a measure of hurricane intensity change;

(ii) Results remain consistent if we use vertical velocity variances on each model level above 20 km, instead of mean variances of vertical velocities of all levels between 20–43 km as the intensity of GWs.

(iii) Moreover, Joaquin is a well-organized hurricane with strong updrafts and large net heating rates in convective bands close to the center. Stratospheric GWs with high intrinsic frequencies and shorter horizontal wavelengths tend to appear close to the hurricane center, while GWs with low intrinsic frequencies and longer horizontal wavelengths are

expected to propagate horizontally further away from the hurricane center (e.g., Alexander et al. 1995; Fritts and Alexander 2003). Therefore, we also tested GWs within 200 km and 300 km of the hurricane center. We found that the above conclusions are robust (i.e., stratospheric GW activity is more frequent and intensive when the hurricane is intensifying than when it is weakening). These results are consistent with the statistical analysis of GW event occurrence frequencies with respect to TC intensity change based on 13.5 years of AIRS observations shown by Hoffmann et al. (2018).

4.4 Time-lagged correlations between stratospheric GWs events and hurricane intensity

Since both TC intensity and features of TC-induced stratospheric GWs individually depend on latent heat release during convection, in this subsection, we analyze correlations between heat release, hurricane intensity, and stratospheric GW activity for the Joaquin case. Our analysis first focuses on GWs with long vertical wavelengths and thus fast vertical phase speeds that may propagate upward to the upper stratosphere in a short time (typically in less than 1 h).

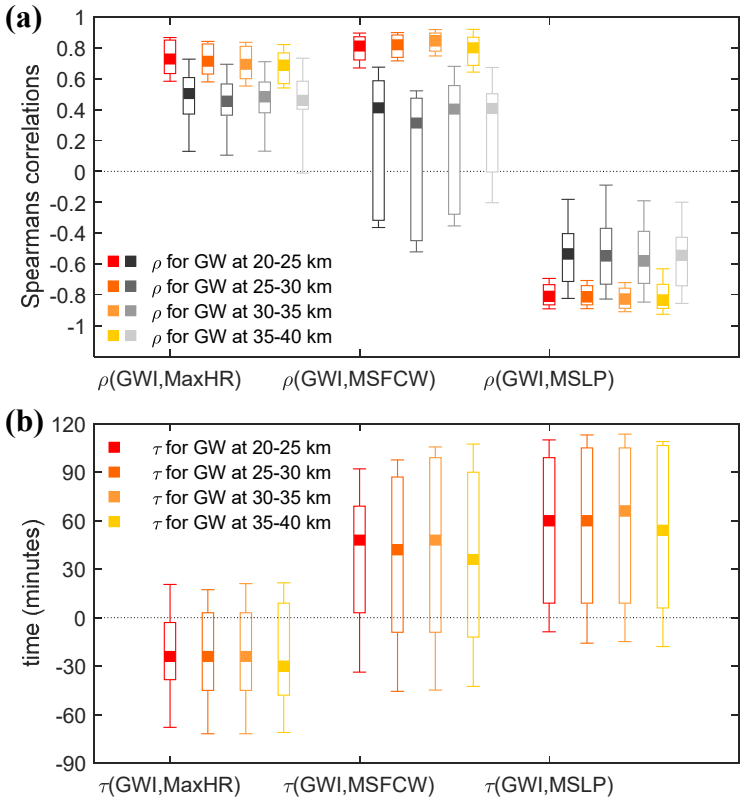

Figure 4. Spearman correlation coefficients and time lag between variable series. Only values that have passed the significance test with 95% are kept. (a) Spearman correlation coefficients ρ between the GWI and MaxHR, MSFCW, and MSLP, respectively. The original ρ is marked in black and grey, and the time-lagged ρ is marked in orange. (b) The "best" time lag τ between GWI and MaxHR, MSFCW, and MSLP, respectively. The box plot displays the minimum, first quartile (25%), median, third quartile (75%), and maximum values.

Mean vertical velocity variances between altitude ranges of 20–25 km, 25–30 km, 30–35 km, and 35–40 km are calculated as a proxy of GW intensity (referred to as GWI

hereafter) at different altitude ranges. According to our simulations, large heat release generally appears between 5–15 km, so we define the maximum heating rate at 5–15 km (referred to as MaxHR hereafter) as an indicator of heat release due to the hurricane. The MSFCW and MSLP are considered as a proxy of hurricane intensity. We split the entire time series of the WRF simulation, excluding the first 12 h of the spin-up period, into independent 6-h segments starting from each model output at a 6-minute interval. That makes 820 cases of 6-h time series of GWI, MaxHR, MSFCW, and MSLP for the statistical analysis. We then calculate the Spearman rank-order correlation coefficients ρ of each pair of time series of GWI versus MaxHR/MSFCW/MSLP. Median values of ρ(GWI, MaxHR), ρ(GWI, MSFCW), and ρ(GWI, MSLP) are about 0.5, 0.4, and −0.6, respectively (Fig. 4a, gray), which indicates a moderate level of correlations between GW activity, heat release, and hurricane intensity. This result agrees with the statistical correlation previously found between stratospheric GW activity and TC intensification based on 13.5 years of AIRS observations of stratospheric GWs (Hoffmann et al., 2018). A sensitivity test with respect to the length of the time series shows that the correlation slightly decreases as the length of the time series increases. For the entire time series, median values of ρ(GWI, MaxHR), ρ(GWI, MSFCW), and ρ(GWI, MSLP) are 0.32, 0.24, and −0.43, respectively (not shown). The correlation for the entire time series is slightly lower than that measured for Hurricane Joaquin by Hoffmann et al. (2018). This difference is reasonable because model output at a 6-minute interval resolves more fluctuations than the 6-hourly observations in Hoffmann et al. (2018). Fluctuations weaken the monotonic relationship between two variable series and thus reduce the Spearman rank-order correlation level.

Considering that there may be a time lag of 0–3 h between a large heat release and TC intensification, as shown in Hazelton et al. (2017), and that GWs take time to propagate to the stratosphere, we searched for the "best" time lag within a time window of ±6 h that produces the most significant time-lagged Spearman rank-order correlation coefficients for each 6-h GWI time series. Correlations significantly increase when the time lag is considered: the median values of time-lagged ρ(GWI, MaxHR), ρ(GWI, MSFCW), and ρ(GWI, MSLP) are about 0.7, 0.8, and −0.8 (Fig. 4a, orange), and the standard deviations of the correlation coefficients considerably decrease. The "best" time lag τ found with this procedure is shown in Fig. 4b. Negative values indicate GW intensity changes after the change of heat release represented by MaxHR, whereas positive values indicate GW intensity varies before the hurricane intensity change as represented by MSFCW and MSLP. The median time lag values show that GW intensity follows the heating rate changes within about 24–30 min, and then the hurricane intensity changes about 36–60 min after the change of GW intensity.

As shown in Fig. 4, GWs are triggered after latent heat release and propagate fast in the vertical direction. They can be observed in the stratosphere even before the hurricane intensity itself increases. However, note that there are large peak-to-peak ranges for the time

lag in Fig. 4b. This variation in the peak-to-peak range shows substantial complexity in the physical relations between latent heat release, hurricane intensity, and GW activity being involved. Therefore, further modeling and observational studies are needed to better understand this complexity and to establish that stratospheric GW activity is not only a proxy but also a reliable predictor of TC intensification. The supplement contains the Spearman correlation coefficients and time lag, same as in Fig. 4 but separately for the intensification and weakening periods.

We conducted sensitivity tests to confirm the robustness of the above results:

(i) The results are consistent if the 99th percentile, median, or mean value of the net heating rates between 5–15 km is used as the indicator of heat release.

(ii) Time windows of ±3 h and ±12 h have been tested for the "best" time lag, and the results agree well with the above results with only minor differences of about 12–18 min in peak-to-peak ranges of the time lag.

(iii) When all stratospheric GWs in the inner domain are considered (up to around 400–500 km from the hurricane center), the correlations between stratospheric GWs and hurricane intensity remain, but the median value of the "best" time lag is around 0. That is, only the fast-propagating GWs have the potential for predicting hurricane intensity.

5 Conclusions

In this study, we performed a mesoscale simulation of Hurricane Joaquin in 2015 using the WRF model to study the correlations between the features of the stratospheric GWs generated by the hurricane and the hurricane intensity. First, the simulated track and intensity of Joaquin were compared with the IBTrACS "best track" data, and the characteristic of the simulated stratospheric GWs was analyzed. It was found that the storm generated spiral GWs and that the GWs rotate and spread anticlockwise away from the hurricane center.

The present study confirms that intensive stratospheric GW activity generated by a hurricane can be a proxy for the intensification of the hurricane itself. Analyses show a clear distinction of GW occurrence frequencies with respect to hurricane intensity change: stratospheric GW activity is more frequent and intensive when the hurricane intensifies rather than when it weakens. This phenomenon is particularly prominent for the strongest GW events. This result agrees with observational results found by Hoffmann et al. (2018) based on 13.5 years of AIRS observations and Wright (2019) based on 17 years of MLS, SABER, and HIRDLS observations of TC-induced gravity waves. Moreover, the correlation between the intensity changes of stratospheric GWs activities and the hurricane is more significant when the time lag is considered.

Measuring the internal structure and dynamics of TCs from space-based infrared sensors is typically not possible because the dense cloud coverage due to the TCs block the view of the instrumentation below cloud top. However, since the stratospheric GW signals that indicate the change of a TC are visible to passive infrared and microwave instruments (e.g., AIRS (Hoffmann and Alexander, 2010; Yue et al., 2013), the Infrared Atmospheric Sounding Interferometer (IASI) (Hoffmann et al., 2014), and MLS (Wright et al., 2014)), it is possible to monitor significant changes in TC intensity by observing GWs with passive

infrared and microwave sounders. This proxy is particularly useful when a cloud canopy obscures the direct view to the TC center for other instruments.

However, it should be noticed that whether intensive stratospheric GW activity can be observed before TC intensification is also largely determined by dynamical and thermal variabilities in the TCs and the effects of the atmospheric background conditions on GW generation and propagation. In addition to latent heating, other factors that may link GW activity and TC intensity, such as the interaction of GWs and TC intensity evolution with the diurnal cycle of TC intensity (Dunion et al., 2014; Evans and Nolan, 2019), will be investigated in future studies.

Acknowledgments

X. Wu is supported by the National Natural Science Foundation of China under grant no. 41975049 and no. 41861134034, and Ground-based Space Environment Comprehensive Monitoring Network (the Chinese Meridian Project II): The Extended Atmospheric Profiling Synthetic Observation System (Tibetan Branch). C. J. Wright and N. P. Hindley are supported by the UK Natural Environment Research Council (NERC) under grant numbers NE/R001391/1 and NE/S00985X/1. C. J. Wright is also supported by a Royal Society University Research Fellowship under grant number UF160545. M. J. Alexander was supported by NSF grant number 1829373. Y. Wang is supported by the second Tibetan Plateau Scientific Expedition and Research Program under grant number 2019QZKK0604 and Key Research Program of Frontier Sciences of CAS under grant number QYZDY-SSW-DQC027.

We thank Dr. K. Görgen from Forschungszentrum Jülich, Dr. J. F. Wu from the University of Science and Technology of China, and Dr. D. Chen from Nanjing University of Information Science and Technology for helpful discussion regarding the WRF model configuration. The authors have no conflicts of interest to declare.

Open Research

The ERA5 reanalysis data (C3S, 2017) were retrieved from ECMWF Meteorological Archival and Retrieval System (https://doi.org/10.24381/cds.adbb2d47; last accessed: 1 November 2021). IBTrACS data were obtained from National Centers for Environmental Information, National Oceanic and Atmospheric Administration (https://doi.org/10.25921/82ty-9e16; last accessed: 1 November 2021).

References

Alexander, M. J., and J. R. Holton (2004), On the spectrum of vertically propagating gravity waves generated by a transient heat source, *Atmos. Chem. Phys.*, *4*(4), 923-932.

Alexander, M. J., J. R. Holton, and D. R. Durran (1995), The Gravity Wave Response above Deep Convection in a Squall Line Simulation, *J. Atmos. Sci.*, *52*(12), 2212-2226.

Beres, J. H., M. J. Alexander, and J. R. Holton (2002), Effects of tropospheric wind shear on the spectrum of convectively generated gravity waves, *J. Atmos. Sci.*, *59*(11), 1805-1824.

366 Beres, J. H., M. J. Alexander, and J. R. Holton (2004), A Method of Specifying the Gravity Wave Spectrum
367 above Convection Based on Latent Heating Properties and Background Wind, *J. Atmos. Sci.*, *61*(3),
368 324-337.
369 Braun, S. A. (2002), A Cloud-Resolving Simulation of Hurricane Bob (1991): Storm Structure and Eyewall
370 Buoyancy, *Mon. Weather Rev.*, *130*(6), 1573-1592.
371 Cecil, D. J., and E. J. Zipser (1999), Relationships between Tropical Cyclone Intensity and Satellite-Based
372 Indicators of Inner Core Convection: 85-GHz Ice-Scattering Signature and Lightning, *Mon. Weather Rev.,*
373 *127*(1), 103-123.
374 Chane-Ming, F., Z. Chen, and F. Roux (2010), Analysis of gravity-waves produced by intense tropical cyclones,
375 *Ann. Geophys.*, *28*(2), 531-547.
376 Chane-Ming, F., S. Jolivet, Y.-A. Liou, F. Jégou, D. Mekies, and J.-S. Hong (2019), Elliptical Structures of
377 Gravity Waves Produced by Typhoon Soudelor in 2015 near Taiwan, *Atmosphere*, *10*(5), 260.
378 Charney, J. G., and A. Eliassen (1964), On the Growth of the Hurricane Depression, *J. Atmos. Sci.*, *21*(1), 68-75.
379 Chow, K. C., K. L. Chan, and A. K. H. Lau (2002), Generation of Moving Spiral Bands in Tropical Cyclones, *J.*
380 *Atmos. Sci.*, *59*(20), 2930-2950.
381 Copernicus Climate Change Service (C3S) (2017), ERA5: Fifth generation of ECMWF atmospheric reanalyses
382 of the global climate. Copernicus Climate Change Service Climate Data Store (CDS), date of access: 14
383 April 2020, https://cds.climate.copernicus.eu/cdsapp#!/home.
384 Dunion, J. P., C. D. Thorncroft, and C. S. Velden (2014), The Tropical Cyclone Diurnal Cycle of Mature
385 Hurricanes, *Mon. Weather Rev., 142*(10), 3900-3919.
386 Emanuel, K. A. (1986), An Air-Sea Interaction Theory for Tropical Cyclones. Part I: Steady-State Maintenance,
387 *J. Atmos. Sci.*, *43*(6), 585-605.
388 Evans, R. C., and D. S. Nolan (2019), Balanced and Radiating Wave Responses to Diurnal Heating in Tropical
389 Cyclone-Like Vortices Using a Linear Nonhydrostatic Model, J. Atmos. Sci., 76(8), 2575-2597.
390 Fritts, D. C., and M. J. Alexander (2003), Gravity wave dynamics and effects in the middle atmosphere, Rev.
391 Geophys., 41(1), 64.
392 Gentry, M. S., and G. M. Lackmann (2010), Sensitivity of Simulated Tropical Cyclone Structure and Intensity
393 to Horizontal Resolution, *Mon. Weather Rev., 138*(3), 688-704.
394 Hazelton, A. T., R. E. Hart, and R. F. Rogers (2017), Analyzing Simulated Convective Bursts in Two Atlantic
395 Hurricanes. Part II: Intensity Change due to Bursts, *Mon. Weather Rev.*, *145*(8), 3095-3117.
396 Hersbach, H., et al. (2020), The ERA5 global reanalysis, *Q. J. R. Meteorol. Soc.*, *146*(730), 1999-2049.
397 Hindley, N. P., N. D. Smith, C. J. Wright, D. A. S. Rees, and N. J. Mitchell (2016), A two-dimensional
398 Stockwell transform for gravity wave analysis of AIRS measurements, *Atmos. Meas. Tech.*, *9*(6),
399 2545-2565.
400 Hindley, N. P., C. J. Wright, N. D. Smith, L. Hoffmann, L. A. Holt, M. J. Alexander, T. Moffat-Griffin, and N.
401 J. Mitchell (2019), Gravity waves in the winter stratosphere over the Southern Ocean: high-resolution
402 satellite observations and 3-D spectral analysis, *Atmos. Chem. Phys.*, *19*(24), 15377-15414.
403 Hodges, K., A. Cobb, and P. L. Vidale (2017), How Well Are Tropical Cyclones Represented in Reanalysis
404 Datasets?, *J. Clim.*, *30*(14), 5243-5264.
405 Hoffmann, L., X. Wu, and M. J. Alexander (2018), Satellite Observations of Stratospheric Gravity Waves
406 Associated With the Intensification of Tropical Cyclones, *Geophys. Res. Lett.* (45).
407 Hoffmann, L., et al. (2019), From ERA-Interim to ERA5: the considerable impact of ECMWF's next-generation
408 reanalysis on Lagrangian transport simulations, *Atmos. Chem. Phys.*, *19*(5), 3097-3124.

409 Holton, J. R., J. H. Beres, and X. Zhou (2002), On the Vertical Scale of Gravity Waves Excited by Localized
410 Thermal Forcing, *J. Atmos. Sci.*, *59*(12), 2019-2023.
411 Hong, S.-Y., and J.-O. J. Lim (2006), The WRF single-moment 6-class microphysics scheme (WSM6), *J.*
412 *Korean Meteor. Soc.*, *42*(2), 129-151.
413 Hong, S.-Y., Y. Noh, and J. Dudhia (2006), A New Vertical Diffusion Package with an Explicit Treatment of
414 Entrainment Processes, *Mon. Weather Rev., 134*(9), 2318-2341.
415 Iacono, M. J., J. S. Delamere, E. J. Mlawer, M. W. Shephard, S. A. Clough, and W. D. Collins (2008), Radiative
416 forcing by long-lived greenhouse gases: Calculations with the AER radiative transfer models, *J. Geophys.*
417 *Res. Atmos.*, *113*(D13).
418 Kain, J. S. (2004), The Kain–Fritsch Convective Parameterization: An Update, *J. Appl. Meteorol.*, *43*(1),
419 170-181.
420 Kim, S.-Y., and H.-Y. Chun (2010), Stratospheric Gravity Waves Generated by Typhoon Saomai (2006):
421 Numerical Modeling in a Moving Frame Following the Typhoon, *J. Atmos. Sci.*, *67*(11), 3617-3636.
422 Knapp, K. R., M. C. Kruk, D. H. Levinson, H. J. Diamond, and C. J. Neumann (2010), The International Best
423 Track Archive for Climate Stewardship (IBTrACS), *Bull. Amer. Meteor. Soc.*, *91*(3), 363-376.
424 Kuester, M. A., M. J. Alexander, and E. A. Ray (2008), A Model Study of Gravity Waves over Hurricane
425 Humberto (2001), *J. Atmos. Sci.*, *65*(10), 3231-3246.
426 Kuo, H. L. (1965), On Formation and Intensification of Tropical Cyclones Through Latent Heat Release by
427 Cumulus Convection, *J. Atmos. Sci.*, *22*(1), 40-63.
428 Miller, S. D., W. C. Straka, J. Yue, S. M. Smith, M. J. Alexander, L. Hoffmann, M. Setvák, and P. T. Partain
429 (2015), Upper atmospheric gravity wave details revealed in nightglow satellite imagery, *Proc. Natl. Acad.*
430 *Sci. USA.*, *112*(49), E6728-E6735.
431 Montgomery, M. T., M. E. Nicholls, T. A. Cram, and A. B. Saunders (2006), A vortical hot tower route to
432 tropical cyclogenesis, J. Atmos. Sci., 63(1), 355-386.
433 Nicholls, M. E., R. A. Pielke, and W. R. Cotton (1991), Thermally Forced Gravity Waves in an Atmosphere at
434 Rest, *J. Atmos. Sci.*, *48*(16), 1869-1884.
435 Nolan, D. S., and J. A. Zhang (2017), Spiral gravity waves radiating from tropical cyclones, *Geophys. Res. Lett.*,
436 *44*(8), 3924-3931.
437 Salby, M. L., and R. R. Garcia (1987), Transient Response to Localized Episodic Heating in the Tropics. Part I:
438 Excitation and Short-Time Near-Field Behavior, *J. Atmos. Sci.*, *44*(2), 458-498.
439 Skamarock, W. C., J. B. Klemp, J. Dudhia, D. O. Gill, M. Barker, K. G. Duda, Y. Huang, W. Wang, and J. G.
440 Powers (2008), A description of the Advanced Research WRF Version 3, Tech. Note
441 NCAR/TN-475+STR, 113 pp., Natl. Cent. for Atmos. Res., Boulder, Colo.
442 Song, I. S., and H. Y. Chun (2005), Momentum flux spectrum of convectively forced internal gravity waves and
443 its application to gravity wave drag parameterization. Part I: Theory, *J. Atmos. Sci.*, *62*(1), 107-124.
444 Stephan, C., and M. J. Alexander (2015), Realistic simulations of atmospheric gravity waves over the
445 continental US using precipitation radar data, *J. Adv. Model. Earth Syst., 7*(2), 823-835.
446 Tratt, D. M., et al. (2018), GHOST: A Satellite Mission Concept for Persistent Monitoring of Stratospheric
447 Gravity Waves Induced by Severe Storms, *Bull. Am. Meteorol. Soc.*, *99*(9), 1813-1828.
448 Wright, C. J. (2019), Quantifying the global impact of tropical cyclone-associated gravity waves using HIRDLS,
449 MLS, SABER and IBTrACS data, *Q. J. R. Meteorol. Soc., 145*(724), 3013-3039.
450 Wright, C. J., N. P. Hindley, L. Hoffmann, M. J. Alexander, and N. J. Mitchell (2017), Exploring gravity wave
451 characteristics in 3-D using a novel S-transform technique: AIRS/Aqua measurements over the Southern
452 Andes and Drake Passage, *Atmos. Chem. Phys.*, *17*(13), 8553-8575.

Wu, J. F., X. H. Xue, H. L. Liu, X. K. Dou, and T. D. Chen (2018), Assessment of the Simulation of Gravity Waves Generation by a Tropical Cyclone in the High-Resolution WACCM and the WRF, *J. Adv. Model. Earth Syst.*, *10*(9), 2214-2227.

Yue, J., L. Hoffmann, and M. Joan Alexander (2013), Simultaneous observations of convective gravity waves from a ground-based airglow imager and the AIRS satellite experiment, *J. Geophys. Res. Atmos.*, *118*(8), 3178-3191.

Yue, J., S. D. Miller, L. Hoffmann, and W. C. Straka (2014), Stratospheric and mesospheric concentric gravity waves over tropical cyclone Mahasen: Joint AIRS and VIIRS satellite observations, *J. Atmos. Sol.-Terr. Phys.*, *119*, 83-90.